Experiments with Human-inspired Behaviors in a Humanoid Robot: Quasi-static Balancing using Toe-off Motion and Stretched Knees

Bernd Henze[1], Máximo A. Roa[1], Alexander Werner[2], Alexander Dietrich[1], Christian Ott[1], Alin Albu-Schäffer[1,3]

***Abstract*— Humanoid robots typically display locomotion patterns that include walking with flat foot-ground contact, and knees slightly bent. However, analysis of human gait indicate that several physiological mechanisms like stretched knees, heel-strike and toe push-off increase the step length and energetic efficiency of locomotion. This paper presents an implementation of two of those mechanisms, namely stretched knees and push-off, on a quasi-static whole-body balancing controller. The influence of such mechanisms on the kinematic capabilities of the DLR humanoid robot TORO is analyzed in different experiments, and their benefits are thoroughly discussed. As a result, the energetic savings of balancing with stretched knees are shown to be of reduced magnitude with respect to the overall power consumption of the robot, and the ability of TORO for negotiating stairs is greatly enhanced.**

I. INTRODUCTION

Humanoid robots can be employed in a large variety of repetitive, physically demanding, or dangerous tasks for a human, as e.g. in service robotics, industrial manufacturing, or disaster management. Most of these applications require locomotion in environments and use of tools initially designed for humans. Humanoid robots resembling a human being in size, proportions, and kinematic structure are in principle more apt for coexisting, collaborating or replacing a human in these challenging tasks.

Operation of humanoid robots in everyday environments requires suitable algorithms for locomotion, capable of dealing with the inherent problem of balancing on two feet or using multiple-contacts. For balancing, recent approaches are focused on achieving whole-body control, which considers the problems of balancing and interacting and manipulating the environment as a single, interconnected challenge. Common approaches for whole-body control can be classified in two different groups, depending on the method for producing the control signals: solving the inverse kinematics/dynamics of the robot [1], [2], [3], [4], or using passivity-based approaches [5], [6], [7]. A subset of the whole-body control frameworks additionally features a hierarchical architecture that allows for multiple control objectives [2], [8].

[1] The authors are with the German Aerospace Center (DLR), Institute of Robotics and Mechatronics, 82234 Wessling, Germany. <firstname>.<lastname>@dlr.de

[2] This author is with the University of Waterloo, N2L 3G1 Waterloo, Canada. <firstname>.<lastname>@uwaterloo.ca

[3] This author is with the Technical University of Munich, Garching, 85748, Germany, <firstname>.<lastname>@dlr.de

This work was supported in part by the European Commission (H2020-ICT-645097, project COMANOID).

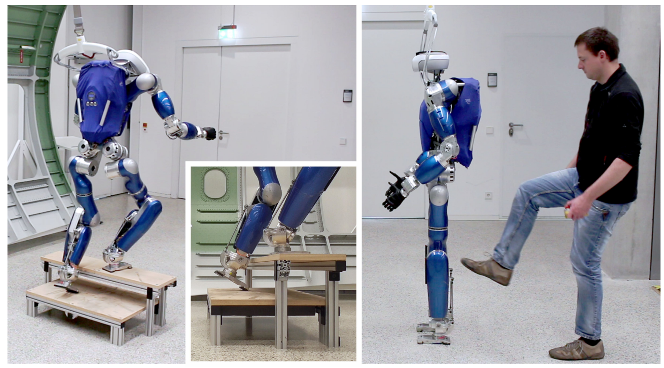

Fig. 1. Human-inspired behaviors on the humanoid robot TORO. Left: Walking up stairs with toe-off motion. Right: Balancing with stretched knees.

For walking, traditional approaches for humanoids rely on motions that keep the foot in flat contact with the ground. However, several approaches have been proposed trying to mimic the human gait on a humanoid robot [9], [10], [11], [12], including phases with stretched knees, heel-strike and toe push-off motions in order to obtain energy-efficient motion patterns, as perceived in human gait [13], [14]. Motivated by those insights, this paper presents an experimental evaluation of stretched knees and toe push-off motions for quasi-static balancing in order to test the potential for reducing the power consumption and for increasing the kinematic workspace during stair climbing. Instead of using additional toe joints as in [15], the push-off motions are performed using line contacts and suitable ankle motions.

The presented experiments exploit our control framework for hierarchical whole-body balancing, presented in [8]. The framework combines passivity-based multi-contact balancing [7] with hierarchical multi-objective control [16]. It was employed in [17] for balancing using contacts scattered all over the body of the robot. In order to handle stretched knees, an adaptation of the hierarchical whole-body balancing controller is presented by adding an additional task, which explicitly regulates the knee angles. The experimental evaluation of the modified controller includes a discussion on the energy savings with respect to the overall power consumption of the humanoid robot TORO (Fig. 1).

The potential advantages of including toe push-off phases into the locomotion pattern of humanoid robots is analyzed in another experiment where the humanoid robot TORO is climbing stairs (Fig. 1). We have previously addressed the problem of stair climbing in [18], where a planning algorithm was combined with our multi-contact balancing controller [7]. As the balancer at that time was not able to perform push-off motions, the robot was only able to master stairs with a height of $5\,\mathrm{cm}$. Including toe-off motions increases the capabilities of the robot by extending the effective length of the rear leg. This leads to an increased hip height, which reduces the required joint torques in the front leg. By including toe push-off phases, we moved from negotiating stairs with step height of $5\,\mathrm{cm}$ and step length of $20\,\mathrm{cm}$ to stairs with step height of $18\,\mathrm{cm}$ and step length of $28\,\mathrm{cm}$, which corresponds to an ordinary staircase in Germany.

The rest of the paper is structured as follows. Section II revises our hierarchical whole-body balancing controller from [8], including the modifications required for stretching the knees and performing push-off motions with the toes. Section III presents the experimental analysis and discussion of the findings. Section IV concludes the paper.

II. Theoretical background

The experimental evaluation presented in this paper utilizes our framework for hierarchical whole-body control previously presented in [8]. As the approach features a hierarchical task prioritization, it can be employed for various applications. Section II-B summarizes the framework and discusses the modifications required for balancing with stretched knees. The modifications to incorporate a toe push-off mechanism are discussed in section II-C. When the framework is used for quasi-static stair climbing, the required task hierarchy becomes identical to our passivity-based approach presented in [7] (section II-D).

A. Dynamic Model

Using a dynamic model with free-floating base is a classical approach in legged humanoid robotics to handle contact transitions. In most cases the hip or trunk are selected as the base link, as they represent the central bodies within the structure of a robot. From a control perspective, it is favorable to select the center of mass (CoM) as base link, as its position is critical for keeping the overall balance. For this reason, a coordinate frame $\mathcal{C}$ located at the CoM but with the same orientation as the hip is introduced in [7]. Let $\boldsymbol{v}_{\mathrm{c}} \in \mathbb{R}^6$ denote the translational and rotational velocity of $\mathcal{C}$. Based on the n joint angles $\boldsymbol{q} \in \mathbb{R}^n$, the dynamics of the humanoid robot is given by

$$\boldsymbol{M}\underbrace{\begin{pmatrix}\dot{\boldsymbol{v}}_{\mathrm{c}}\\ \ddot{\boldsymbol{q}}\end{pmatrix}}_{\dot{\boldsymbol{\nu}}}+\boldsymbol{C}\underbrace{\begin{pmatrix}\boldsymbol{v}_{\mathrm{c}}\\ \dot{\boldsymbol{q}}\end{pmatrix}}_{\boldsymbol{\nu}}+\underbrace{\begin{pmatrix}m\boldsymbol{g}_0\\ \boldsymbol{0}\end{pmatrix}}_{\boldsymbol{g}}=\underbrace{\begin{pmatrix}\boldsymbol{0}\\ \boldsymbol{\tau}\end{pmatrix}}_{\boldsymbol{u}}+\boldsymbol{\tau}_{\mathrm{ext}}, \tag{1}$$

where $\boldsymbol{M} \in \mathbb{R}^{(6+n)\times(6+n)}$ and $\boldsymbol{C} \in \mathbb{R}^{(6+n)\times(6+n)}$ denote the inertia and Coriolis/centrifugal matrix, respectively. The velocities of the CoM frame $\boldsymbol{v}_{\mathrm{c}}$ and of the joints $\dot{\boldsymbol{q}}$ are combined into $\boldsymbol{\nu} \in \mathbb{R}^{6+n}$. The influence of gravity is taken into account by $\boldsymbol{g} \in \mathbb{R}^{6+n}$, containing the gravitational acceleration $\boldsymbol{g}_0 \in \mathbb{R}^6$ and the total mass m of the robot[1].

[1]Note that $\boldsymbol{g}_0$ is six-dimensional, as it also contains the rotational DoFs. The structure of $\boldsymbol{g}$ is caused by the choice of $\mathcal{C}$ as base frame (see [5]).

TABLE I
TASK HIERARCHIES OF THE APPLIED BALANCING CONTROLLERS.

	Task Wrench $\boldsymbol{F}_i$	
Level i	With Knee Task	Without Knee Task
1	$\boldsymbol{\tau}_{\mathrm{knee}}$	$(\boldsymbol{F}_{\mathrm{c}}^T\ \boldsymbol{F}_{\mathrm{bal}}^T\ \boldsymbol{F}_{\mathrm{int}}^T)^T$
2	$\boldsymbol{F}_{\mathrm{bal}}$	$\boldsymbol{\tau}_{\mathrm{pose}}$
3	$(\boldsymbol{F}_{\mathrm{c}}^T\ \boldsymbol{F}_{\mathrm{int}}^T)^T$	–
4	$\boldsymbol{\tau}_{\mathrm{pose}}$	–

The control input $\boldsymbol{u}$ acts only on the n joints of the robot via the control torques $\boldsymbol{\tau} \in \mathbb{R}^n$. The influence of external disturbances is given by the generalized forces $\boldsymbol{\tau}_{\mathrm{ext}} \in \mathbb{R}^{6+n}$.

B. Hierarchical Balancing Control

We used a hierarchical whole-body controller in [17] in order to balance in over-constrained contact situations, typically arising from contacts scattered all over the body of the robot. The first task within the hierarchy was given by the physical contact constraint, forcing all other tasks to take place in the null-space of the Jacobian matrix related to this physical constraint. In order to balance with stretched knees, we propose to use a similar approach by employing the hierarchy specified in the left column of Table I: The first priority level ($i = 1$) comprises an explicit task for stabilizing the knee joints in a stretched position using the compliance control $\boldsymbol{\tau}_{\mathrm{knee}} \in \mathbb{R}^2$. Note that the controller can also deal with the knees in any other given configuration, although stretching the knees appears to be the most logical choice to reduce the power consumption and/or extend the workspace of the robot (see Sec. III). Although stretching the knees is not a physical constraint as in [17] but rather a constraint invoked by a controller, all the other tasks (level 2 to 4) need to be operated in the null space of the Jacobian matrix for task 1. The second task comprises the so-called *balancing end-effectors*, which are used to generate a suitable set of contact wrenches $\boldsymbol{F}_{\mathrm{bal}} \in \mathbb{R}^{m_{\mathrm{bal}}}$ in order to support the robot. The remaining end-effectors will be referred to as *interaction end-effectors* because they can be used to perform a potential interaction task such as manipulating an object. The interaction end-effectors are stabilized by Cartesian compliances stacked into the wrench vector $\boldsymbol{F}_{\mathrm{int}} \in \mathbb{R}^{m_{\mathrm{int}}}$. Together with a Cartesian compliance $\boldsymbol{F}_{\mathrm{c}} \in \mathbb{R}^6$ regulating the CoM frame $\mathcal{C}$, they form the task with priority level $i = 3$. The fourth task consists of a compliance with control action $\boldsymbol{\tau}_{\mathrm{pose}} \in \mathbb{R}^n$ to regulate the pose in joint space, in order to deal with redundant robots.

The control law can be deduced in a similar way as in [8]. All r tasks are defined by a task Jacobian $\boldsymbol{J}_i \in \mathbb{R}^{m_i\times(n+6)}$ mapping the velocity in configuration space $\boldsymbol{\nu} \in \mathbb{R}^{n+6}$ to the task velocities $\dot{\boldsymbol{x}}_i \in \mathbb{R}^{m_i}$:

$$\dot{\boldsymbol{x}}_i = \boldsymbol{J}_i\boldsymbol{\nu} \qquad \forall i = 1\ldots r. \tag{2}$$

Based on the task definition, null space base matrices $\boldsymbol{Z}_i \in \mathbb{R}^{m_i\times(6+n)}$ and a null space projector $\boldsymbol{N}_i \in \mathbb{R}^{(6+n)\times(6+n)}$ can be computed as detailed in [16]. The null space projector

$$\boldsymbol{N}_i = \boldsymbol{I} - (\boldsymbol{J}_{i-1}^{\mathrm{aug}})^T(\boldsymbol{J}_{i-1}^{\mathrm{aug}})^{\boldsymbol{M}+,T} \tag{3}$$

maps the control action on level i onto the null space of all task Jacobian matrices with a higher priority $(1\ldots(i-1))$, which are stacked into $\boldsymbol{J}_{i-1}^{\mathrm{aug}}$. Herein, $\boldsymbol{J}_{i-1}^{\boldsymbol{M}+}$ denotes the dynamically consistent pseudo-inverse [16]. Applying these steps to the particular task hierarchy given in Table I yields

$$\boldsymbol{u} = \begin{pmatrix} \boldsymbol{0} \\ \boldsymbol{\tau} \end{pmatrix} = \begin{pmatrix} m\boldsymbol{g}_0 \\ \boldsymbol{0} \end{pmatrix} + \boldsymbol{\tau}_\mu - \boldsymbol{\Xi}\boldsymbol{F} \tag{4}$$

with $\boldsymbol{\tau}_\mu \in \mathbb{R}^{(6+n)}$ compensating for coupling terms within the matrix $\boldsymbol{C}$. The latter is necessary for achieving a dynamic decoupling between the tasks, but can be omitted during motions with moderate velocities [16]. The task wrenches are stacked into $\boldsymbol{F} = \left(\boldsymbol{\tau}_{\text{knee}}^T\ \boldsymbol{F}_{\text{bal}}^T\ \boldsymbol{F}_{\text{int}}^T\ \boldsymbol{F}_{\text{c}}^T\ \boldsymbol{\tau}_{\text{pose}}^T\right)^T \in \mathbb{R}^\sigma$ and the mapping $\boldsymbol{\Xi} \in \mathbb{R}^{(6+n)\times\sigma}$ is partitioned into

$$\boldsymbol{\Xi} = \begin{bmatrix} \boldsymbol{J}_{\text{knee}}^T & \boldsymbol{N}_2\boldsymbol{J}_{\text{bal}}^T & \boldsymbol{N}_3\boldsymbol{J}_3^T & \boldsymbol{N}_4\boldsymbol{J}_4^T \end{bmatrix} = \begin{bmatrix} \boldsymbol{\Xi}_u \\ \boldsymbol{\Xi}_l \end{bmatrix}. \tag{5}$$

Here, $\boldsymbol{\Xi}_u \in \mathbb{R}^{6\times\sigma}$ maps $\boldsymbol{F}$ onto the DoF of the base, while $\boldsymbol{\Xi}_l \in \mathbb{R}^{n\times\sigma}$ provides a mapping onto the n joint torques.

In order to account for the under-actuation of the base, $\boldsymbol{F}_{\text{bal}}$ must be chosen such that $m\boldsymbol{g}_0 = \boldsymbol{\Xi}_u\boldsymbol{F}$ holds by minimizing the quadratic cost function

$$\min_{\boldsymbol{F}_{\text{bal}}} \left(\boldsymbol{F}_{\text{bal}} - \boldsymbol{F}_{\text{bal}}^{\text{def}}\right)^T \boldsymbol{Q} \left(\boldsymbol{F}_{\text{bal}} - \boldsymbol{F}_{\text{bal}}^{\text{def}}\right) \tag{6}$$

with respect to

$$m\boldsymbol{g}_0 = \boldsymbol{\Xi}_u\boldsymbol{F} \tag{7}$$

and to the contact model

$$\boldsymbol{A}_{\text{bal}}\boldsymbol{F}_{\text{bal}} \leq \boldsymbol{b}_{\text{bal}}. \tag{8}$$

The cost function minimizes the deviation of the balancing wrenches from a default wrench distribution $\boldsymbol{F}_{\text{bal}}^{\text{def}} \in \mathbb{R}^{m_{\text{bal}}}$. The contact model (8) consists of a polyhedron defined via $\boldsymbol{A}_{\text{bal}} \in \mathbb{R}^{\rho\times m_{\text{bal}}}$ and $\boldsymbol{b}_{\text{bal}} \in \mathbb{R}^\rho$, and accounts for unilaterality, friction and the location of the center of pressure (CoP) of each contact in order to prevent the balancing end-effectors from lifting off, sliding, or tilting (see [7] for details). After obtaining $\boldsymbol{F}_{\text{bal}}$ from (6), the control torque $\boldsymbol{\tau}$ is computed via $\boldsymbol{\tau} = -\boldsymbol{\Xi}_l\boldsymbol{F}$ according to (4).

Inserting (4) into (1) leads to a decoupled closed-loop dynamics

$$\boldsymbol{\Lambda}\dot{\boldsymbol{v}} + \boldsymbol{\mu}\boldsymbol{v} + \begin{pmatrix} \boldsymbol{F}_1 \\ \boldsymbol{Z}_2\boldsymbol{J}_2^T\boldsymbol{F}_2 \\ \vdots \\ \boldsymbol{Z}_r\boldsymbol{J}_r^T\boldsymbol{F}_r \end{pmatrix} = \bar{\boldsymbol{J}}^{-T}\boldsymbol{\tau}_{\text{ext}} \tag{9}$$

based on local, hierarchy-consistent null space velocities $\boldsymbol{v} = \left(\boldsymbol{v}_1^T \ldots \boldsymbol{v}_r^T\right)^T$ given by $\boldsymbol{v} = \bar{\boldsymbol{J}}\boldsymbol{\nu}$. The computation of $\bar{\boldsymbol{J}}$ and $\bar{\boldsymbol{J}}^{-1} = \left[\boldsymbol{J}_1^{\boldsymbol{M}+}, \boldsymbol{Z}_2^T, \ldots, \boldsymbol{Z}_r^T\right]$ is detailed in [16], [8]. Let us consider the case in which there are no external disturbances acting on the robot except for the balancing wrenches $\boldsymbol{F}_{\text{bal}}^{\text{ext}}$, then the simplification

$$\bar{\boldsymbol{J}}^{-T}\boldsymbol{\tau}_{\text{ext}} = \begin{bmatrix} \boldsymbol{J}_{\text{knee}}^{\boldsymbol{M}+,T}\boldsymbol{J}_{\text{bal}}^T \\ \boldsymbol{Z}_2\boldsymbol{J}_{\text{bal}}^T \\ \boldsymbol{0} \\ \boldsymbol{0} \end{bmatrix} \boldsymbol{F}_{\text{bal}}^{\text{ext}} \tag{10}$$

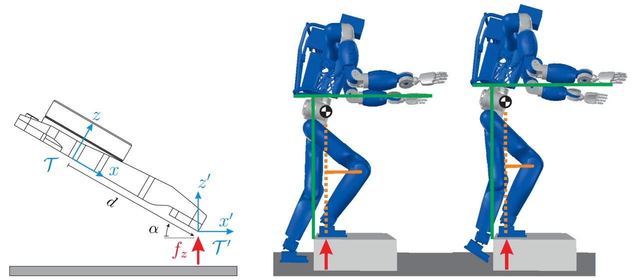

(a) Modified end-effector frame $\mathcal{T}'$.

(b) Impact on hip height (green) and lever arms (orange) governing the joint torques.

Fig. 2. Toe-off motion of the rear leg during stair climbing.

can be made. As expected, the external balancing wrenches $\boldsymbol{F}_{\text{bal}}^{\text{ext}}$ act on the balancing task (level $i = 2$) and are counteracted by the commanded balancing wrenches $\boldsymbol{F}_{\text{bal}}$. But $\boldsymbol{F}_{\text{bal}}^{\text{ext}}$ acts also on task level $i = 1$, which represents a significant disturbance to the knee task considering that $\boldsymbol{F}_{\text{bal}}^{\text{ext}}$ supports the weight of the robot. Thus, we propose to compensate for the disturbance by choosing

$$\boldsymbol{\tau}_{\text{knee}} = \boldsymbol{\tau}_{\text{knee}}^{\text{cpl}} + \boldsymbol{J}_{\text{knee}}^{\boldsymbol{M}+,T}\boldsymbol{J}_{\text{bal}}^T\boldsymbol{F}_{\text{bal}}, \tag{11}$$

which consists of a compliance $\boldsymbol{\tau}_{\text{knee}}^{\text{cpl}}$ stabilizing the knee angles, and a compensation term using the commanded balancing wrenches $\boldsymbol{F}_{\text{bal}}$. Based on this choice, the closed-loop dynamics simplifies to

$$\boldsymbol{\Lambda}\dot{\boldsymbol{v}} + \boldsymbol{\mu}\boldsymbol{v} + \begin{pmatrix} \boldsymbol{\tau}_{\text{knee}}^{\text{cpl}} + \boldsymbol{J}_{\text{knee}}^{\boldsymbol{M}+,T}\boldsymbol{J}_{\text{bal}}^T\boldsymbol{F}_{\text{bal}} \\ \boldsymbol{Z}_2\boldsymbol{J}_{\text{bal}}^T\boldsymbol{F}_{\text{bal}} \\ \boldsymbol{Z}_3\boldsymbol{J}_3^T\boldsymbol{F}_3 \\ \boldsymbol{Z}_4\boldsymbol{J}_4^T\boldsymbol{F}_4 \end{pmatrix} = \begin{bmatrix} \boldsymbol{J}_{\text{knee}}^{\boldsymbol{M}+,T}\boldsymbol{J}_{\text{bal}}^T \\ \boldsymbol{Z}_2\boldsymbol{J}_{\text{bal}}^T \\ \boldsymbol{0} \\ \boldsymbol{0} \end{bmatrix} \boldsymbol{F}_{\text{bal}}^{\text{ext}}. \tag{12}$$

Note that due to the use of $\boldsymbol{F}_{\text{bal}}$ in (11) instead of $\boldsymbol{F}_{\text{bal}}^{\text{ext}}$, the external wrenches are not fully compensated, but the disturbance is reduced from $\boldsymbol{F}_{\text{bal}}^{\text{ext}}$ to the difference $\boldsymbol{F}_{\text{bal}} - \boldsymbol{F}_{\text{bal}}^{\text{ext}}$. As a consequence, this introduces a new coupling from task 2 onto task 1. This coupling could only be avoided by compensating for the real contact wrenches $\boldsymbol{F}_{\text{bal}}^{\text{ext}}$. However, that would inevitably raise the well-known problems of measuring external forces (e.g. algebraic loops).

C. Modifications for Toe Push-Off Motions

In order to allow for toe push-off motions, we modify the presented control approach by shifting and rotating the end-effector frames of the feet as shown in Fig. 2a. During flat contact the end-effector frame is located in its default configuration $\mathcal{T}$ underneath the ankle, with the x-axis pointing to the front and the z-axis being perpendicular to the sole of the foot. In order to incline the foot, the frame is first moved by an offset d to the front edge of the contact area before the frame is rotated by an angle α, such that the z-axis is no longer perpendicular to the sole but to the ground floor. In theory, the resulting line contact should be able to transmit horizontal forces in x'- and y'-directions, as well as torques about the x'- and z'-axis. However, it is questionable if the contact is stable enough to provide those forces and torques, because an inclination of the foot usually happens in situations with rather low vertical load. Therefore, we propose to model the contact as a point contact only providing a vertical force $\boldsymbol{f}_z$ for balancing, which can be achieved by assigning only the translational z'-direction to the balancing end-effectors. The remaining 5 DoFs are allocated to the interaction end-effectors, which has as an advantage that these DoFs are stabilized by a Cartesian compliance including the inclination of the foot, thus significantly increasing the robustness against slipping and tilting. Note that this method can as well be used to perform a heel strike by shifting the end-effector frame to the back of the foot.

D. Relation to the HRO-Balancing Controller

The stair climbing experiment presented in section III-B utilizes a rather general task hierarchy without an explicit task for stretching the knees (see right column of Table I): The tasks for the CoM, the interaction and the balancing end-effectors are arranged on the same priority level ($i = 1$). As before, the lowest priority level ($i = 2$) comprises a compliance $\boldsymbol{\tau}_{\text{pose}}$ in joint space. But instead of projecting $\boldsymbol{\tau}_{\text{pose}}$ in the null space of $\boldsymbol{J}_1^{\text{aug}} = \left[\, \boldsymbol{J}_{\text{c}}^T \; \boldsymbol{J}_{\text{bal}}^T \; \boldsymbol{J}_{\text{int}}^T \,\right]^T$, it is projected onto the null space of the Sub-Jacobian $\tilde{\boldsymbol{J}}_1^{\text{aug}} = \boldsymbol{J}_1^{\text{aug}} \left[\, \boldsymbol{0}_{n\times 6} \; \boldsymbol{I}_{n\times n} \,\right]^T$, which only accounts for the motion of the n DoFs in joint space. The corresponding null space projector is given by

$$\tilde{\boldsymbol{N}} = \boldsymbol{I} - \tilde{\boldsymbol{J}}^T \tilde{\boldsymbol{J}}^{\tilde{\boldsymbol{M}}+,T} \tag{13}$$

with $\tilde{\boldsymbol{M}} = \left[\, \boldsymbol{0}_{n\times 6} \; \boldsymbol{I}_{n\times n} \,\right] \boldsymbol{M} \left[\, \boldsymbol{0}_{n\times 6} \; \boldsymbol{I}_{n\times n} \,\right]^T$. Although this null space projector does not lead to a dynamic decoupling of the tasks [16], it has proven itself to be very robust even in extreme configurations such as stair climbing. In consequence, the task hierarchy used for stair climbing results in the same control law as our “HRO-balancing controller”, previously published in [7].

III. Experimental Evaluation

The experimental validation of the approaches for balancing with stretched knees and toe-off motions is performed with the torque-controlled robot TORO. The robot has a height of $1.74\,\text{m}$ and weighs $76.4\,\text{kg}$ [19], [20]. It features 25 DoF in total (not counting the hands and the neck), which are located in the legs, arms, and hip. These joints are based on the technology of the DLR-KUKA LBR (lightweight robot arm), and can be operated in both position and torque control modes. The controllers are implemented in MATLAB/Simulink, and qpOASES [21] is used to solve the constrained quadratic optimization problem (6) to (8).

A. Balancing with Stretched Knees

In order to evaluate the disturbance rejection of the two task hierarchies discussed in sections II-B and II-D, the humanoid robot was brought into a configuration with stretched knees (Fig. 1), and received two consecutive pushes of about the same magnitude at the left and right knees. The results are shown in Fig. 3 for the controller with and without an explicit knee task (see Table I). The pushes result in a knee flexion of up to 20° and 15°, respectively. The main difference between both task hierarchies is that after the pushes, the one with an explicit task for stretching the knees shows a smaller static deviation than the one without a knee task (HRO-Balancer). The latter regulates the knee flexion only indirectly via the CoM compliance, which is supposed to preserve the CoM height. However, due to the singular configuration produced by the stretched knees, the resulting wrench $\boldsymbol{F}_{\text{c}}^{\text{cpl}}$ at the CoM does not generate sufficient knee torque to overcome joint friction. Therefore, the hierarchical controller is not able to return the robot into the fully stretched configuration without an explicit task for the knee angles.

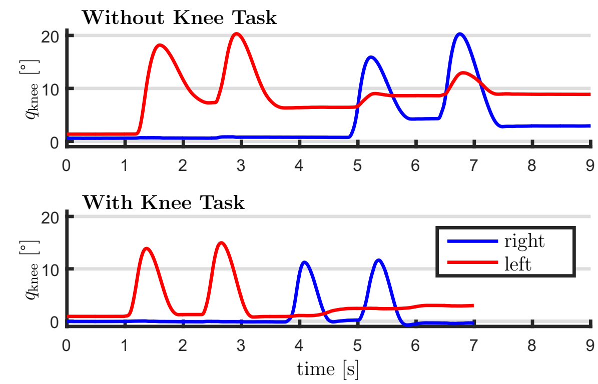

Fig. 3. Disturbance rejection for both hierarchical controllers when TORO receives consecutive pushes at the left and right knee.

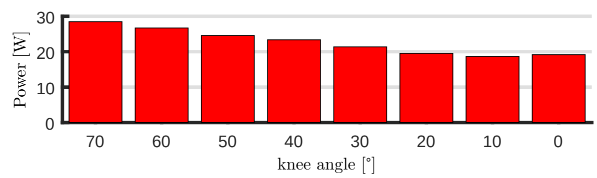

Fig. 4. Power consumption of the legs during static balancing as a function of the knee flexion.

The most common argument for balancing with stretched knees presented in literature is the reduced power consumption [9], [11], [12]. In order to validate this argument, the robot was placed in eight different configurations, each one with a different knee angle in the range of 0° to 70°. In each configuration, the robot was controlled by the balancing controller featuring an explicit knee task (section II-B), and the power consumption of both legs was measured[2]. In most cases TORO is operated with a knee angle of about 40°, e.g. during walking. As the measurements in Fig. 4 indicate, the power consumption could be reduced by $4\,\text{W}$ by stretching the knees. Considering a knee angle of 70° as reference, stretching the knees would lead to a reduction of $9\,\text{W}$. Therefore, we can confirm that on TORO the stretched knees reduce the power consumption. However, one must also consider that besides the legs, a humanoid robot comprises many more electrical components, e.g. arm

[2]Note that the measurement comprises the consumption of the motors, the power electronics, and the electronics for low-level joint control.

joints, sensors, and computers. In the case of TORO, the overall power consumption is around $350\,\mathrm{W}$ during static balancing, which is mostly caused by the three computers used for control and vision processing. Therefore, stretching the knees can reduce the overall power consumption by only 2.5%. A similar analysis was conducted in [11] for dynamic walking, which revealed a significant improvement of the cost of transport by incorporating human-inspired motion patterns. But for static balancing, our results imply that more efficient computers and algorithms have a potentially higher impact on the energy consumption, compared to optimizing the posture of the robot. Besides this, stretching the knees results in a reduced agility of the hip, which can be of relevance for performing a manipulation task with the upper body. Therefore, it is probably more favorable to bend the knees during static balancing instead of stretching them. As our experiment indicates, the difference regarding the power consumption is small enough to be neglected.

B. Stair Climbing with Toe Push-off Motion

The second experiment discusses the advantages of toe-off motions to increase the kinematic workspace during stair climbing utilizing the task hierarchy without an explicit task for the knees from Sec. II-D (HRO-balancer). For this purpose, TORO was commanded to quasi-statically go up two stairs with step height of $18\,\mathrm{cm}$ and step length of $28\,\mathrm{cm}$, which corresponds to an ordinary staircase in Germany. A series of snapshots of the motion is given in Fig. 5. The motion can be divided into nine phases P1 to P9, depending on the contacts used for balancing: double stance ("d"), right foot only ("r"), and left foot only ("l"). For instance, the robot uses a double stance during the phases P3 and P7, in which the right foot is placed on the next step while the left foot still remains on the previous one. During the sub-phases P3a and P7a, both feet are in flat contact with the ground. In the sub-phases P3b and P7b, the robot performs a toe push-off motion with the left/rear foot, in order to increase its kinematic capability.

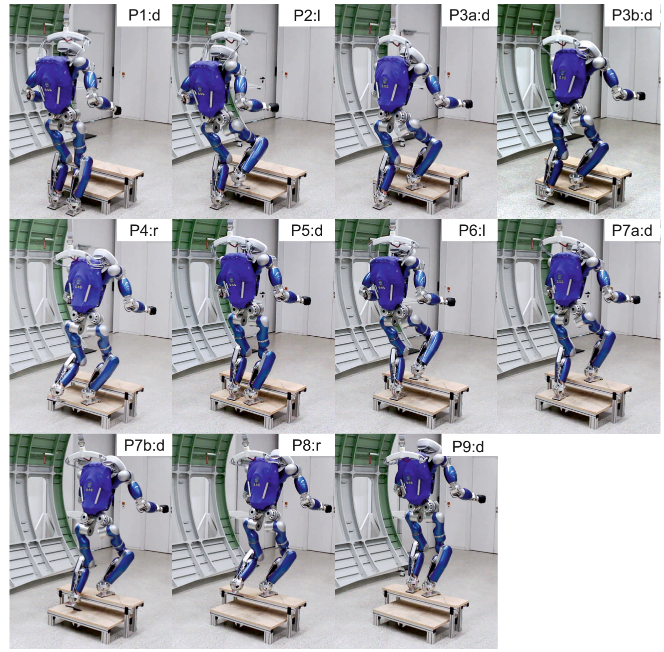

Fig. 5. TORO climbing two stairs with a step height of $18\,\mathrm{cm}$ and step length of $28\,\mathrm{cm}$. The motion of the robot is divided into nine phases, P1 to P9, according to the contacts used for balancing: double stance (d), right foot (r), and left foot (l).

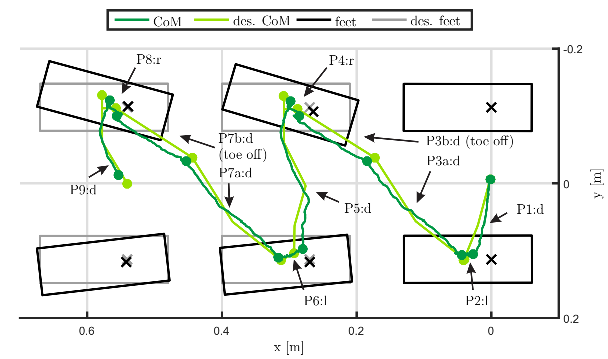

Fig. 6. Footprints during stair climbing.

The top view is given in Fig. 6, which shows the footprints and the CoM oscillating between the right and the left foot. The controller achieves a sufficient tracking of the CoM considering a moderate stiffness[3] for the CoM compliance $\boldsymbol{F}_{\mathrm{c}}^{\mathrm{cpl}}$ and joint friction. Note that the controller tends to place the feet slightly rotated outwards, whereby the right foot is more affected than the left one. The reason for this is that the robot always moves first the right leg to the front in order to place it on the next step, which brings the right leg into a rather twisted configuration involving all six joints. Therefore, the motion of the right leg is more affected by friction than the left/rear one, which could be counteracted by increasing the rotational stiffness of the compliances regulating the feet. However, the orientation error is not problematic at all as the robot always shifts its weight on top of the stance-foot, regardless of the orientation. The experiment, shown in the attached video, displays a rather slow motion for going upstairs, as the robot is close to its hardware limitations regarding kinematics, joint torques, and contact model.

The advantage of performing a toe-off motion with the left foot is that it extends the effective length of the rear leg, and therefore the kinematic capability of the robot. As shown in Fig. 2b, this extension allows the robot to increase the height of the hip (green), which leads to a reduced knee flexion. Let us consider the exact moment in time when the robot is about to lift the rear foot, which means that the entire weight of the robot is on the forward leg. Fig. 2b shows that an increased height of the hip reduces the lever arm responsible for the torque in the right knee (orange), which results in a reduction of the right knee torque. In order to analyze this effect, we conducted a simulation study with TORO performing the stair climbing experiment with and without toe-off motion. Without toe-off, the required torque in the knee is at 96% of the maximum torque possible at this joint, which is too close to the limit to be tested on

[3]The parametrization of the compliances is identical to the one in [7].

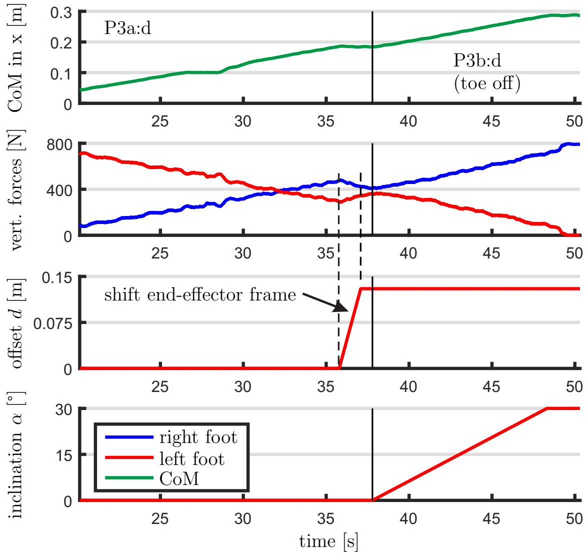

Fig. 7. Detailed analysis of the toe-off motion during phase P3.

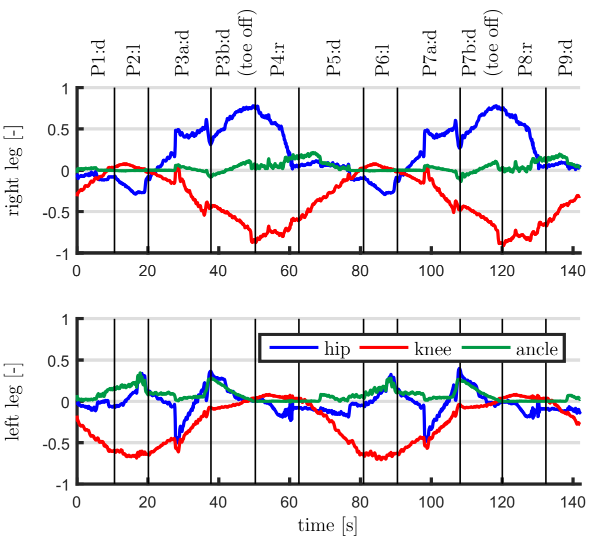

Fig. 8. Normalized joint torques $\boldsymbol{\tau}/\boldsymbol{\tau}_{\max}$ during stair climbing.

the real robot, considering joint friction and measurement noise. By performing the toe-off motion, the knee torque can be reduced to 76% of the maximum torque, which leaves enough margin for an experiment. Therefore, climbing stairs of this particular height is only possible by using a toe-off motion in order to extend the length of the rear leg, resulting in a higher hip location and thereby lower knee torque.

Fig. 7 shows the measurements recorded during phase P3 of the experiment. The CoM is shifted by $24\,\mathrm{cm}$ to the front in order to move it from a location on top of the rear foot to a location on top of the forward foot. This shift results in the weight of the robot being transferred from the left to the right leg. At the end of phase P3a, the end-effector frame of the rear foot is shifted from underneath the ankle to the forefront of the foot (see $\mathcal{T} \rightarrow \mathcal{T}'$ in Fig. 2a) in order to prepare the toe-off motion in phase P3b. Shifting the frame of the rear foot to the front reduced the lever arm between the end-effector frame and the CoM, which partially transfers back the load from the right/forward to the left/rear leg. Finally, in phase P3b the inclination angle of the rear foot is slowly ramped to 30° in order to generate the toe-off motion.

The consequences of inclining the foot can also be seen in the normalized joint torques given in Fig. 8 (± 1 indicates the maximum torque for each joint). At the beginning of phase P3b and P7b, the torque in the left ankle is relatively high due to the lever arm between the shifted end-effector frame $\mathcal{T}'$ and the ankle joint (Fig. 2a). With an increasing inclination of the foot, the lever arm is reduced, which also lowers the torque in the ankle joint. As soon as the robot enters the next phase (P4 and P8) by lifting the rear/left foot, the entire load is on the right leg. As a result, the right knee and the right hip joint are strained up to 78% and 92% of their maximum torque, which is barely within the limits of the robot. This emphasizes again that without toe-off motion the robot would not be able to move upstairs. Only by extending the effective length of the rear leg, we can achieve joint torques that are within the hardware limits of the robot.

IV. CONCLUSION

This work presents an experimental analysis of stretched knees and toe push-off motions for quasi-static balancing in order to increase the capabilities of humanoid robots by adopting human-inspired behaviors. In order to balance with stretched knees, we modified our hierarchical whole-body control algorithm [8] by adding a task that explicitly regulates the knee angle. The key is to design the task torque such that it accounts for the contact wrenches, which act as a disturbance on the knee task. In [11], it was shown that human-inspired motions such as stretching the knees can improve the power consumption significantly. This work presents an experimental evaluation of the power consumption during static balancing with the robot TORO. Although the experiments confirm the hypothesis that the power consumption of the legs can be reduced by stretching the knees, they also revealed that the power consumption of the complete robot is dominated by the onboard computers, and that modifying the knee angle can only save up to 2.5% of the overall consumption. Thus, we recommend to not only consider the posture of the robot for reducing the power consumption, but also to explore more efficient algorithms and computation hardware in the future.

The second experiment on stair climbing revealed that toe push-off motions can be used to increase the kinematic capability of the rear leg by increasing its effective length. This allows to move the hip into a higher location, which reduces the knee flexion of the front leg. Decreasing the knee angle leads to a reduction of the knee torque, which was one of the limiting factors in our previous work on stair climbing [18], allowing only a step height of $5\,\mathrm{cm}$. By incorporating toe push-off motions into our whole-body control framework, TORO was able to master a regular German staircase with step height of $18\,\mathrm{cm}$. In the future, we plan to extend our work to more dynamic walking.

REFERENCES

[1] B. J. Stephens and C. G. Atkeson, "Dynamic balance force control for compliant humanoid robots," in *IEEE/RSJ Int. Conf. on Intelligent Robots and Systems*, 2010, pp. 1248–1255.

[2] L. Sentis, J. Park, and O. Khatib, "Compliant control of multicontact and center-of-mass behaviors in humanoid robots," *IEEE Trans. on Robotics*, vol. 26, no. 3, pp. 483–501, 2010.

[3] L. Righetti, J. Buchli, M. Mistry, M. Kalakrishnan, and S. Schaal, "Optimal distribution of contact forces with inverse-dynamics control," *Int. J. of Robotics Research*, vol. 32, no. 3, pp. 280–298, 2013.

[4] M. Mistry, J. Buchli, and S. Schaal, "Inverse dynamics control of floating base systems using orthogonal decomposition," in *IEEE Int. Conf. on Robotics and Automation*, 2010, pp. 3406–3412.

[5] S.-H. Hyon, J. G. Hale, and G. Cheng, "Full-body compliant human-humanoid interaction: Balancing in the presence of unknown external forces," *IEEE Trans. on Robotics*, vol. 23, no. 5, pp. 884–898, 2007.

[6] C. Ott, M. A. Roa, and G. Hirzinger, "Posture and balance control for biped robots based on contact force optimization," in *IEEE-RAS Int. Conf. on Humanoid Robots*, 2011, pp. 26–33.

[7] B. Henze, M. A. Roa, and C. Ott, "Passivity-based whole-body balancing for torque-controlled humanoid robots in multi-contact scenarios," *Int. J. of Robotic Research*, vol. 35, no. 2, pp. 1522–1543, 2016.

[8] B. Henze, A. Dietrich, and C. Ott, "An approach to combine balancing with hierarchical whole-body control for legged humanoid robots," *IEEE Robotics and Automation Letters*, vol. 1, no. 2, pp. 700–707, 2016.

[9] Y. Ogura, K. Shimomura, H. Kondo, A. Morishima, T. Okubo, S. Momoki, H. Lim, and A. Takanishi, "Human-like walking with knee stretched, heel-contact and toe-off motion by a humanoid robot," in *IEEE/RSJ Int. Conf. on Intelligent Robots and Systems*, 2006, pp. 3976–3981.

[10] Z. Li, N. G. Tsagarikis, D. G. Caldwell, and B. Vanderborght, "Trajectory generation of straightened knee walking for humanoid robot iCub," in *Int. Conf. on Control Automation Robotics Vision*, 2010, pp. 2355–2360.

[11] J. Reher, A. Hereid, S. Kolathaya, C. Hubicki, and A. D.Ames, "Algorithmic foundations of realizing multi-contact locomotion on the humanoid robot DURUS," in *Workshop on the Algorithmic Foundations of Robotics (WAFR)*, 2016.

[12] R. J. Griffin, G. Wiedebach, S. Bertrand, A. Leonessa, and J. Pratt, "Straight-leg walking through underconstrained whole-body control," in *IEEE Int. Conf. on Robotics and Automation*, 2018, pp. 5747–5754.

[13] J. B. dec. M. Saunders, V. T. Inman, and H. D. Eberhart, "The major determinants in normal and pathological gait," *The Journal of Bone and Joint Surgery*, vol. 35-A, no. 3, pp. 543–558, 1953.

[14] D. Torricelli, J. Gonzalez, M. Weckx, R. Jiménez-Fabián, B. Vanderborght, M. Sartori, S. Dosen, D. Farina, D. Lefeber, and J. L. Pons, "Human-like compliant locomotion: state of the art of robotic implementations," *Bioinspiration & Biomimetics*, vol. 11, no. 5, p. 051002, 2016.

[15] K. Nishiwaki, S. Kagami, Y. Kuniyoshi, M. Inaba, and H. Inoue, "Toe joints that enhance bipedal and fullbody motion of humanoid robots," in *IEEE Int. Conf. on Robotics and Automation*, 2002, pp. 3105–3110.

[16] A. Dietrich, *Whole-Body Impedance Control of Wheeled Humanoid Robots*, ser. Springer Tracts in Advanced Robotics, 2016, vol. 116.

[17] B. Henze, A. Dietrich, M. A. Roa, and C. Ott, "Multi-contact balancing of humanoid robots in confined spaces: Utilizing knee contacts," in *IEEE/RSJ Int. Conf. on Intelligent Robots and Systems*, 2017, pp. 679–704.

[18] A. Werner, B. Henze, D. A. Rodriguez, J. Gabaret, O. Porges, and M. A. Roa, "Multi-contact planning and control for a torque-controlled humanoid robot," in *IEEE/RSJ Int. Conf. on Intelligent Robots and Systems*, 2016, pp. 5708–5715.

[19] J. Englsberger, A. Werner, C. Ott, B. Henze, M. A. Roa, G. Garofalo, R. Burger, A. Beyer, O. Eiberger, K. Schmid, and A. Albu-Schäffer, "Overview of the torque-controlled humanoid robot TORO," in *IEEE-RAS Int. Conf. on Humanoid Robots*, 2014, pp. 916–923.

[20] B. Henze, A. Werner, M. A. Roa, G. Garofalo, J. Englsberger, and C. Ott, "Control applications of TORO - a torque controlled humanoid robot," in *IEEE-RAS Int. Conf. on Humanoid Robots*, 2014, p. 841.

[21] H. J. Ferreau, H. G. Bock, and M. Diehl, "An online active set strategy to overcome the limitations of explicit MPC," *Int. J. Robust and Nonlinear Control*, vol. 18, no. 8, pp. 816–830, 2008.